

Association and Dissociation of an Aqueous Amphiphile at Elevated Temperatures

D. T. Bowron^{*,†,‡} and J. L. Finney[‡]

ISIS Facility, Rutherford Appleton Laboratory, Chilton, Didcot OX11 0QX, United Kingdom, and Department of Physics and Astronomy, University College London, Gower Street, London WC1E 6BT, United Kingdom

Received: May 15, 2007; In Final Form: June 13, 2007

The hydrophobic interaction is often thought to increase with increasing temperature. Although there is good experimental evidence for decreased aqueous solubility and increased clustering of both nonpolar and amphiphilic molecules as temperature is increased, the detailed nature of the changes in intermolecular interactions with temperature remain unknown. By use of isotope substitution neutron scattering difference measurements on a 0.04 mole fraction solution of *tert*-butanol in water as the solute clustering passes through a temperature maximum, the changes in local intermolecular structures are examined. Although, as expected, the solute molecules cluster through increased contact between their nonpolar head groups with the exclusion of water, the detailed geometry of the mutual interactions changes as temperature increases. As the clustering breaks up with further temperature increase, the local structures formed do not mirror those that were found in the low-temperature dispersed system: the disassembly process is not the reverse of assembly. The clusters formed by the solute head groups are reminiscent of structures that are found in systems of spherical molecules, modulated by the additional constraint of near-maximal hydrogen bonding between the polar tails of the alcohol and the solvent water. Although the overall temperature behavior is qualitatively what would be expected of a hydrophobically driven system, the way the system resolves the competing interactions and their different temperature dependencies is complex, suggesting it could be misleading to think of the aggregation of aqueous amphiphiles solely in terms of a hydrophobic driving force.

Introduction

The hydrophobic interaction is generally thought to increase in strength with increasing temperature. In appropriate systems, free energy changes as temperature increases have been interpreted as an increase in the strength of the hydrophobic interaction, with the rate of increase falling to a plateau.¹ Experimental measurements² and computer simulation³ both show an aqueous solubility minimum for the inert gases Ar, Kr, and Xe, and for methane, between about 70 and 100 °C, results that are consistent with the hydrophobic interaction going through a maximum at these temperatures.

One expected structural consequence of this increased interaction is an increase in longer-range correlations between solute molecules. Evidence of such longer-range correlations has come from techniques such as light scattering^{4,5} and small-angle X-ray scattering⁶ measurements on *tert*-butanol–water solutions. Although *tert*-butanol is an amphiphile, possessing both polar and nonpolar moieties, its thermodynamic behavior is generally thought to be dominated by hydrophobic interactions.⁷ With respect to “pure” nonpolar molecules, computer simulation calculations of methane in water show an increase in the solute–solute contacts, which reach a maximum at 66 °C and then fall as the molecules begin to disaggregate.⁸ Even by 103 °C, however, there is still significantly more solute aggregation than at room temperature. Other simulations of ethane in water also show a rise in solute aggregation with increasing temperature, reaching a maximum at about 50 °C.⁹

In this calculation, a further temperature increase to 75 °C resulted in a first-neighbor distribution similar to that at room temperature.

The behavior of aqueous solutions of both nonpolar molecules and amphiphiles with increasing temperature is of intense interest chemically, biologically, and to the biotechnology industry. As it is generally believed that hydrophobic interactions are a significant—some would argue the major—driving force stabilizing the native structures of proteins, the variation of this interaction with temperature is relevant to the high-temperature stability of these biologically active molecules and of particular interest with respect to thermophilic enzymes. With the discovery of organisms growing at up to 113 °C, much interest in protein stability has focused on proteins from these organisms, many of which are stable above 100 °C in vitro. Part of this interest is biotechnological and includes efforts to engineer increased stability into industrially useful proteins.

This experimental and computational evidence of increasing aggregation of both nonpolar and amphiphilic molecules as temperature is raised, followed by a further disaggregation as temperature increases further, is consistent with the purported temperature dependence of the hydrophobic interaction. However, questions have been raised as to whether the explanation for the observed aggregation should be placed at the door of the hydrophobic interaction. For example, the free energy term used by Ben Naim¹ as a measure of hydrophobic interaction strength has been queried by Pratt and Chandler,¹⁰ who argue that there is no microscopic interpretation that is compatible with the claim that the hydrophobic interaction increases in strength as the temperature is raised.

It is therefore appropriate to examine at the molecular level the detailed nature of the aggregation and subsequent disag-

* Corresponding author: e-mail D.T.Bowron@rl.ac.uk.

[†] Rutherford Appleton Laboratory.

[‡] University College London.

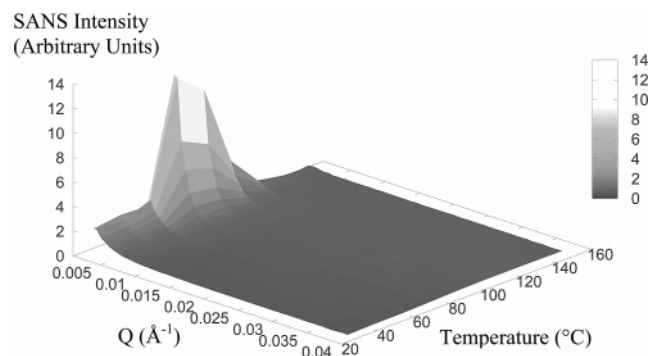


Figure 1. Small-angle neutron scattering (SANS) intensity for a 0.04 mole fraction solution of *tert*-butanol in water as a function of temperature between 25 and 150 °C.

gregation of solute molecules as an aqueous solution passes through the purported hydrophobic maximum. We report here the results of a temperature-dependent study of the aggregation and subsequent disaggregation in water of *tert*-butanol. Although the behavior observed indeed appears to be consistent with what would be expected from the normal hydrophobic interaction considerations, the detailed molecular structures of the solute clusters formed suggest a behavior of significantly greater subtlety. As both proteins and micellar structures are built from amphiphilic rather than nonpolar subunits, the results are of relevance to discussions of the dependence of protein stability and micelle formation on temperature.

Recent Relevant Work: Small-Angle Neutron Scattering.

In order to study the mesoscopic structural fluctuations from the viewpoint of the alcohol molecules, small-angle neutron scattering (SANS) data have been reported from mixtures of protiated *tert*-butanol, (CH₃)₃COH in D₂O.¹¹ To investigate the temperature dependence of the long-range structural correlations, data were collected between 20 and 106 °C so as to cover the range over which hydrophobic effects are thought to pass through a maximum.

The SANS results obtained for a 0.04 mole fraction solution of *tert*-butanol are shown in Figure 1.¹¹ This concentration is close to that at which the sharp minimum in the partial molar volume of *tert*-butanol in *tert*-butanol–water mixtures occurs,¹² a concentration that has been consequently associated with a maximization of the hydrophobic effects operating in this mixture.⁷ When the usual scattering vector Q is defined as $4\pi(\sin \theta)/\lambda$, where 2θ is the scattering angle of neutron radiation of wavelength λ , the small-angle scattering increases only below a Q of 0.015 Å⁻¹, suggesting that correlation lengths of upward of several hundred angstroms exist in this system. The temperature dependence of this scattering is quite remarkable. The signal increases to a maximum at ~80 °C and then falls away with increasing temperature, reaching a value lower than that at room temperature by around 140 °C. A simple interpretation of these observations suggests that as the temperature is increased from ambient, the degree of mesoscopic length scale solution structure increases from that at which the liquid mixture appears almost completely homogeneous at the length scales probed. The correlations indicated by the peak near 80 °C then fall away above this temperature until a second, comparatively homogeneous solution state is reached above 120 °C.

SANS is by its nature a low-resolution technique. In this case, it shows only that long-range structural correlations increase and then fall as temperature is increased over the 25–140 °C range. In the absence of higher resolution structural data, the precise structural origin of the long-range correlations is unclear. Though the isotopic contrast enhancement allows us to assume

that in some way these long-range correlations relate directly to the distribution of alcohol molecules within the system, it does not tell us whether the scattering is from individual large structural entities that have the characteristic large correlation length or whether it is from long-range correlations between smaller structural entities: is the solution demixed on the longer length scales, or are microclusters of alcohol molecules correlating over large distances? The fact that the scattering functions are flat between 0.015 and 0.04 Å⁻¹ seems to suggest that if the latter hypothesis is valid, the size of the small alcohol clusters must be less than about 150 Å as there is no obvious small-angle scattering signal in the range from there up to >400 Å.

By use of isotope substitution neutron diffraction, the room-temperature baseline intermolecular structure of dilute solutions of *tert*-butanol in water has already been characterized for 0.02^{13,14} and 0.06^{15,16} mole fraction concentrations. These results show that in the more dilute solution the alcohol molecules tend to remain either as free molecules or as linear alcohol dimers interacting through head-to-head nonpolar group to nonpolar group contacts.^{13,14} At the higher concentration of 0.06 mole fraction, the degree of orientational ordering between associated alcohol molecules is more diverse, with the average cluster size for alcohol association being 3–4 molecules.¹⁶ The molecules in these molecular clusters still tend to interact through nonpolar group to nonpolar group interactions. However, there are no equivalent data for the intermediate 0.04 mole fraction concentration to help understand the changes observed in the SANS experiments. We report here such measurements on this system at three temperatures: at room temperature (25 °C), at a temperature corresponding to the maximum of clustering indicated by the SANS measurements (80 °C), and finally at a higher temperature at which the SANS data indicate a falling off in the degree of clustering (106 °C).

Experimental Section

Neutron scattering was used to measure the interference differential scattering cross section, $F(Q)$, of a 0.04 mole fraction solution of *tert*-butanol in water at temperatures of 25, 80, and 106 °C. This interference differential scattering cross section is also known as the total structure factor and contains information about the structural correlations between pairs of atoms within the system, weighted respectively by the concentrations, c , and scattering lengths, b , of each atomic species:

$$F(Q) = \sum_{\alpha \leq \beta} (2 - \delta_{\alpha\beta}) c_{\alpha} c_{\beta} b_{\alpha} b_{\beta} [S_{\alpha\beta}(Q) - 1] \quad (1)$$

The sum is over all atomic species that can each in turn be denoted by the subscript α or β , and $\delta_{\alpha\beta}$ is the Kronecker δ function to avoid double counting of like terms within the summation. $S_{\alpha\beta}(Q)$ are the partial structure factors that describes the pairwise interactions between atoms as a function of the magnitude of the scattering vector Q , defined earlier.

To better evaluate the structural information contained in a structure factor, it is useful to Fourier transform the function from its dependence on the scattering vector to a dependence on the radial distance between atoms, r . The transformation, here directly related to the partial structure factors, takes the form

$$[g_{\alpha\beta}(r) - 1] = \frac{1}{2\pi^2 \rho} \int_0^{\infty} Q^2 [S_{\alpha\beta}(Q) - 1] \frac{\sin Qr}{Qr} dQ \quad (2)$$

where ρ is the atomic density of the sample and $g_{\alpha\beta}(r)$ is the

pair distribution function that represents the pairwise distribution of atoms of type β around atoms of type α , or vice versa, as a function of their separation r . Naturally, if only a single neutron diffraction experiment is performed, it is only possible to evaluate the total pair distribution function $g(r)$, as there are insufficient experimental constraints to allow determination of the individual partial pair distribution terms.

For hydrogen-containing systems, it is possible to take advantage of the different neutron scattering properties of hydrogen ($b_H = -3.74$ fm) and deuterium ($b_D = 6.67$ fm) to address the challenge of separating the specific pairwise structural contributions that make up the total structure factor. By performing a series of experiments on samples that have the same chemical composition but are isotopically distinct, it is possible to isolate the correlations between atom sites in terms of up to three more informative pair distribution functions.¹⁷ These correlation functions respectively address (i) interactions between the isotopically substituted sites themselves, (ii) interactions between the substituted and the nonsubstituted sites, and (iii) interactions between just the nonsubstituted atomic sites. By use of the established structural modeling technique summarized in the following section, these correlation functions enable us to access the specific site–site pair correlation functions $g_{\alpha\beta}(r)$.

To investigate the structure of the 0.04 mole fraction aqueous solution of *tert*-butanol, a series of five neutron scattering measurements on chemically identical but isotopically distinct samples have been performed. Isotopically speaking, the samples investigated were (1) $(CD_3)_3COD$ in D_2O , (2) $(CH_3)_3COH$ in H_2O , (3) a 1:1 mixture of $(CD_3)_3COD$ and $(CH_3)_3COH$ in a 1:1 mixture of D_2O and H_2O , (4) $(CD_3)_3COH$ in H_2O , and (5) a 1:1 mixture of $(CD_3)_3COH$ and $(CD_3)_3COD$ in a 1:1 mixture of D_2O and H_2O . Solutions 1–3 weight the structural sensitivity of the experiment toward correlations between the alcohol and water hydrogen sites, while solutions 1, 4, and 5 weight the structural sensitivity toward correlations between the water hydrogen (and alcohol hydroxyl hydrogen) sites.

Each sample was prepared by weight and transferred to “null-scattering” $Ti_{0.68}Zr_{0.32}$ alloy cells that have a composition that makes no structural contribution to the coherent neutron scattering signal. The cells were sealed to vacuum with a poly-(tetrafluoroethylene) (PTFE) O-ring. The sample dimensions, delimited by the cell walls, were 35 mm height \times 35 mm width \times 1 mm thickness. Neutron scattering measurements were performed by use of the small-angle neutron diffractometer for amorphous and liquid samples (SANDALS) at the ISIS Facility, Rutherford Appleton Laboratory, U.K.. The five isotopically distinct samples were mounted on the instrument’s automatic sample changer that allows control of the sample temperature in the range from 0 to 110 °C with a stability better than ± 0.5 °C. Measurements were made for sample temperatures of 25, 80, and 106 °C, and time-of-flight neutron scattering data were collected over an angular range from 3° to 40° by use of arrays of lithium-doped ZnS scintillation detectors over neutron wavelengths in the range from 0.05 to 2.5 Å. This instrument configuration gives a corresponding Q -range of 0.2–50 Å^{−1} that can be used in the structural analysis. As all the cells were completely filled and sealed at room temperature, that is, leaving no expansion volume, the atomic density used throughout the analysis was 0.1 atom Å^{−3}.

The data were corrected for instrument and cell background scattering, multiple scattering, and absorption by use of the Gudrun codes that evolved from the widely used Atlas package.¹⁸ The data were placed on an absolute scale by normaliza-

tion to the scattering of a known vanadium standard, and corrections for self-scattering and inelastic scattering were performed by the methods outlined by Soper and Luzar.¹⁹

Structural Modeling. To gain insight into the detailed three-dimensional structure of the system as a function of temperature, the data were analyzed by the technique of empirical potential structure refinement (EPSR).²⁰ This technique results in a full three-dimensional structure reconstruction that allows access to all the site–site pair distribution functions that combine to give the experimentally observed total distribution functions and is also consistent with the known chemistry of the molecule and the solution density. Within this analysis framework, the molecular structures are constrained to maintain chemically reasonable geometries. This constraint brings a significant but often overlooked advantage: weakly weighted pair distribution functions in the neutron scattering data become accessible with enhanced reliability if their location within a molecular unit is highly correlated with more strongly scattering functional groups. This characteristic of the analysis methodology plays a central role in this study of the *tert*-butanol–water system. The critically important tertiary carbon sites, which define the centers of the alcohol molecules, make only a weak contribution to the measured structure factors. However, as the location of tertiary carbon sites is highly correlated with the location of the alcohol molecules’ three methyl groups and their associated strongly neutron scattering hydrogen/deuterium sites, it is possible to extract the tertiary carbon correlations with a comparable reliability to the methyl hydrogen site correlations.

In the EPSR technique, a classical Monte Carlo simulation of the system is generated that is then used to produce ensemble average information of key structural parameters, constrained to be consistent with the available experimental scattering data. Initially the simulation is equilibrated by use of a set of standard reference potentials based on Lennard-Jones parameters and charges. The simulation is then perturbed through the development and incorporation of potentials of mean force derived from the available experimental data. Under this scheme the Monte Carlo simulation is effectively driven into agreement with the available structural information, and once experimental agreement is obtained, accumulation of ensemble average information is commenced. The partial pair distribution functions and other structural data of interest can then be extracted.

The simulations used to model the 0.04 mole fraction *tert*-butanol–water solutions were initialized by placing 24 alcohol molecules and 576 solvent molecules into a box of side length 27.5 Å, corresponding to the experimental atomic density of 0.1 atom Å^{−3}. To facilitate the discussion of structural information, the following atom labels are used for distinguishable sites on the *tert*-butanol and water molecules: CC for the tertiary carbon (“central carbon”) site of the alcohol molecule, C for the methyl group carbon sites, M for the methyl group hydrogen sites, O for the alcohol hydroxyl group oxygen, H for the alcohol hydroxyl group hydrogen, OW for the water oxygen sites, and HW for the water hydrogen sites. The initial Lennard-Jones parameters and charges used to seed the simulation are given in Table 1.

The fully corrected interference differential scattering cross sections for the five samples at the three investigated temperatures are shown in Figure 2, along with the EPSR structural models refined to the experimental data. Overall the quality of the fit is good, though some deviation at low Q is seen in some of the fits for the samples containing hydrogen as opposed to deuterium. In general these deviations are found to correspond to low-frequency components that would contribute to real space

TABLE 1: Lennard-Jones, Charge, and Atomic Mass Parameters^a

| atom type | ϵ , kJ mol ⁻¹ | σ , Å | M , amu | q , e |
|-----------|-----------------------------------|--------------|-----------|---------|
| CC | 0.209 | 3.80 | 12 | 0.265 |
| C | 0.607 | 3.96 | 12 | 0.000 |
| M | 0.000 | 1.35 | 1 | 0.000 |
| O | 0.712 | 3.07 | 16 | -0.700 |
| H | 0.000 | 1.35 | 1 | 0.435 |
| OW | 0.650 | 3.16 | 16 | -0.8476 |
| HW | 0.000 | 0.00 | 2 | 0.4238 |

^a Used for the reference potentials that seed the empirical potential structure refinement model of the *tert*-butanol + water solution.

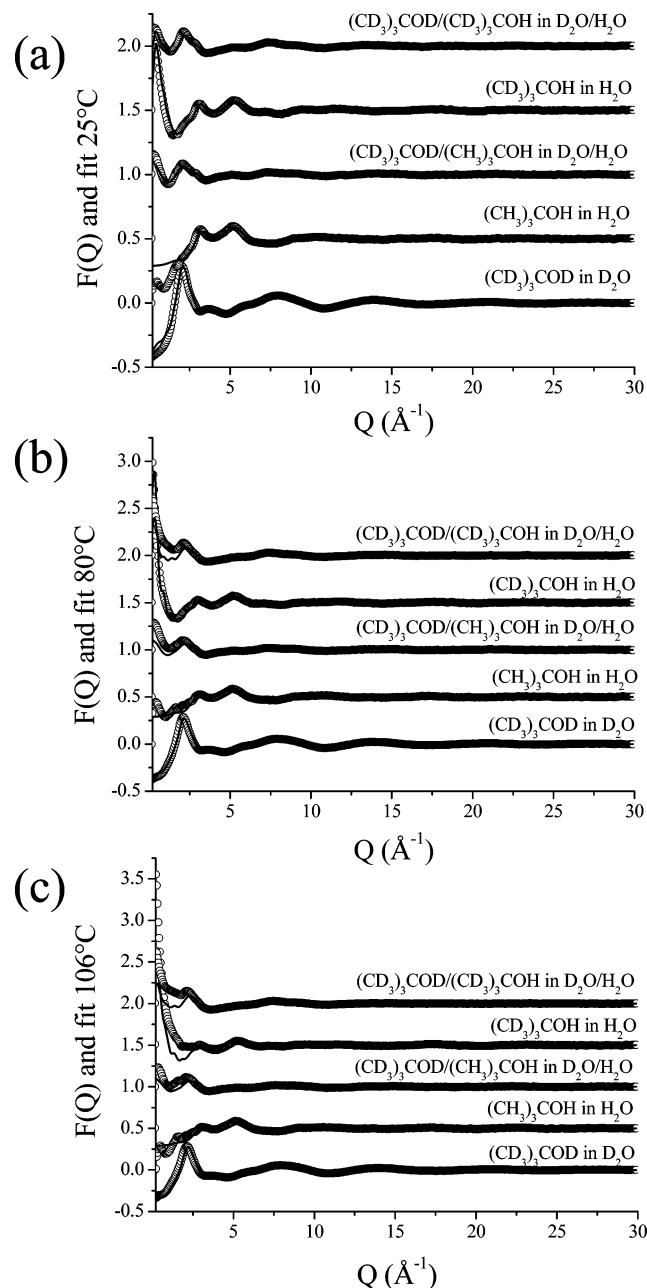


Figure 2. Experimentally measured interference differential scattering cross sections for H/D-labeled 0.04 mole fraction aqueous solutions of *tert*-butanol (○) and EPSR model fits (—) at (a) 25, (b) 80, and (c) 106 °C.

features at unphysically short interatomic distances and generally result from background components that remain following the final data corrections for inelastic scattering processes. The EPSR analysis method was specifically developed to minimize

bias from such unphysical data features that would plague more traditional data interpretation schemes.

Results

Solute Clustering. Figure 3 shows instantaneous snapshots of the solute taken from the EPSR simulations that are consistent with the experimental results at the three temperatures. The 80 °C temperature coincides with the maximum in the SANS data (Figure 1), while at 106 °C the SANS intensity has begun to fall. The snapshots show a clear increase in solute clustering in the 80 °C solution. At the highest temperature, obviously large clusters such as the one to the left in the 80 °C snapshot have broken down somewhat, qualitatively consistent with the observed reduction in the small-angle scattering.

To quantify this temperature-dependent clustering and to look in detail at the kinds of intermolecular interactions occurring between solute and solute and between solute and solvent, we need to examine the appropriate experimentally consistent partial radial distributions that are obtained from the EPSR procedure. The 28 partial radial distribution functions that characterize the structure of these solutions are shown in Figures 4–7.

From the central carbon–central carbon radial distribution function of Figure 7, we can extract estimates of the solute–solute coordination numbers. Using a cutoff distance criterion of 7.5 Å, a distance that corresponds to the first minimum in this function at each of the three temperatures, we obtain the coordination number distributions shown in Figure 8. These distributions show that as we go from 25 to 80 °C, there is a growth of larger clusters at the expense of smaller ones. As the temperature increases further, the fraction of larger clusters has begun to decrease to the advantage of an increased number of smaller clusters. The general impression of enhanced clustering at the SANS maximum, followed by a subsequent cluster breakdown with a further temperature increase, is supported quantitatively by these high-resolution results.

The interesting question arises as to the detailed molecular-level structures of these clusters. What sort of interactions are occurring in this clustering and the subsequent apparent dispersion? Can we understand the underlying chemistry of the intermolecular contacts? How might polar and nonpolar interactions participate in these contacts, and how might these results relate to the hydrophobic interaction? We can begin to answer some of these questions by examining further the relevant distribution functions obtained from the EPSR refinement of the experimental results.

Interactions with the *tert*-Butanol Polar Tail Group at Room Temperature. Considering first the possibility of *tert*-butanol–*tert*-butanol association through direct hydrogen bonding, the coordination number of 0.1 ± 0.1 obtained from the relevant O–O partial radial distribution function (see Table 2) shows an effective absence of such interactions at 25 °C. This is consistent with the negligible population of hydrogen-bonded solute dimers found in earlier measurements on this and other aqueous alcohol systems.^{14,15,21} That earlier work showed that the OH group on the *tert*-butanol interacts mainly with solvent molecules, and examining the alcohol oxygen to water oxygen (O–OW) partial radial distribution function (RDF) for the 0.04 mole fraction concentration (Figure 6) leads us to the same conclusion that the solvent water is strongly preferred by the alcohol's OH group. Interestingly, however, in the 0.04 mole fraction solution, the coordination number of 2.8 ± 0.3 (Table 2) is some 10% larger than those obtained for both lower and higher 0.02 and 0.06 concentrations.^{14,16} [Note that the range quoted is an indication of the range of coordination numbers

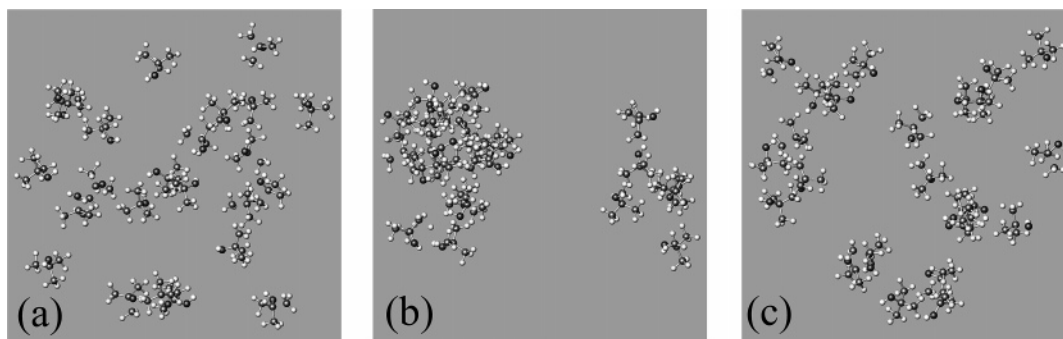


Figure 3. Snapshots of the simulation box for a 0.04 mole fraction solution of *tert*-butanol in water at temperatures of (a) 25, (b) 80, and (c) 106 °C. To highlight the structural heterogeneities in the solutions, the water molecules have been deleted from the viewport.

found in the ensembles; it is not a standard error.] The results obtained for this 0.04 concentration are consistent with the solute–solvent hydrogen bonding being essentially maximized, the OH group being generally thought capable of making three good hydrogen bonds.

Interactions with the *tert*-Butanol Nonpolar Head Group at Room Temperature. Again referring to the coordination numbers in Table 2, from the central carbon–water oxygen values, we find that there are, on average, 26 ± 1 first-neighbor waters out to the first deep minimum at 6.5 Å in the partial radial distribution (Figure 4). Looking at the coordination number relating to neighboring *tert*-butanol molecules interacting through nonpolar to nonpolar head group contacts (CC–CC) shows an average of 1.8 ± 0.4 . Both these values are similar to those obtained for the lower 0.02 concentration, implying that both the hydration of the nonpolar head group and the average environments of the nonpolar head group are quantitatively similar to those reported earlier.^{13,14}

Orientations of Head Group Interactions. We can interrogate the EPSR ensembles to obtain information on the detailed nature of the interactions between contacting *tert*-butanol molecules. To do this, we need to break the spherical averaging involved in obtaining the partial radial distributions and look initially at the spatial density function,²² which describes the positioning of neighboring solute molecules around the central molecule. This is essentially similar to finding the most probable latitudes and longitudes of the neighboring *tert*-butanol molecules on an imaginary sphere centered on the central carbon of the central molecule, as illustrated in Figure 9. The reference orientation of the central *tert*-butanol molecule is with its nonpolar head group pointing upward and its polar tail pointing down.

Figure 10 shows an average over ϕ_1 of the *tert*-butanol–*tert*-butanol spatial density function. The brightest lobe centered on 12 o'clock tells us that most of the neighboring *tert*-butanol molecules “cap” the central molecule; the less intense, broader features centered on about 3 o'clock and 9 o'clock show that there are some intermolecular contacts coming in from the side of the molecule. The lack of any significant observable intensity near 6 o'clock reflects the lack of dimerization through the polar tail that was discussed earlier.

We can now look at the molecules that are represented in the bright zones of this spatial density function and look at their orientations. To describe these orientations, we use appropriate orientational pair correlation functions,²³ for which we use the coordinate set shown in Figure 9. For the neighboring molecules that contribute to the bright 12 o'clock lobe in Figure 10 ($\theta_1 = 0$), we show in Figure 11 the orientations of the neighboring *tert*-butanol molecules through a θ_m map. The brightest lobe near 9–10 o'clock tells us that the dominant relative orientation

is as depicted in the left of Figure 11. The capping molecule has its z-axis (its O–CC vector) oriented at about 90° to that of the central molecule, a configuration we refer to below as “T-like”. This orientation is unexpected: for both lower and higher concentrations, earlier work shows the dominant relative orientation to be one with the two O–CC vectors pointing along each other, an “in-line” configuration that maximizes the nonpolar surface contacts between two *tert*-butanol molecules.^{13–16}

The results of the room temperature measurements on the 0.04 mole fraction solution lead us to the following conclusions.

First, there is a small but significant microscopic clustering observed, an effect that has been observed earlier in both higher and lower concentrated solutions of both *tert*-butanol and other alcohols.^{14,15,21} The degree of clustering is approximately the same as that at the lower 0.02 concentration.

With respect to the intermolecular solute–solute interactions in these clusters at room temperature, as for other concentrations that have been studied of both *tert*-butanol and other alcohols, there is no significant alcohol–alcohol H-bonding between neighbouring solute molecules. Rather, the polar tail alcohol group interacts preferentially with solvent water. There is an indication that the polar group in the 0.04 mole fraction solution is effectively hydrogen-bond-saturated, with on average about three water molecules interacting with the polar group. This is a greater degree of hydrogen bonding than is found at either lower or higher concentrations.

The solute–solute interactions are, as found in earlier work at different concentrations,^{13–16} predominantly through contacting nonpolar head groups. However, there is a major difference between the most probable relative orientations of the contacting molecules at this 0.04 concentration: whereas the previously observed most probable orientation is an in-line 180° mutual orientation, the 0.04 mole fraction solution contacts are dominated by the near-right-angle T-like mutual orientation. We might draw attention here to the fact that the 0.04 mole fraction concentration is close to that at which there is a deep minimum in the partial molar volume of the solute (see Figure 10 in Franks and Desnoyers⁷), a concentration that has perhaps consequently been conceptually linked with some kind of maximization of the hydrophobic interaction in this system.

Structural Evolution upon Increasing Temperature. Figure 7 shows the temperature dependence of the 0.04 mole fraction central carbon–central carbon partial radial distribution function. As we go from the 25 to the 80 °C SANS maximum, the first peak increases, reflecting the increase in average first-neighbor solute–solute coordination from 1.8 to 2.8 (Table 2). The further increase in temperature to 106 °C sees the first peak in the partial radial distribution begin to fall, with a reduction in the

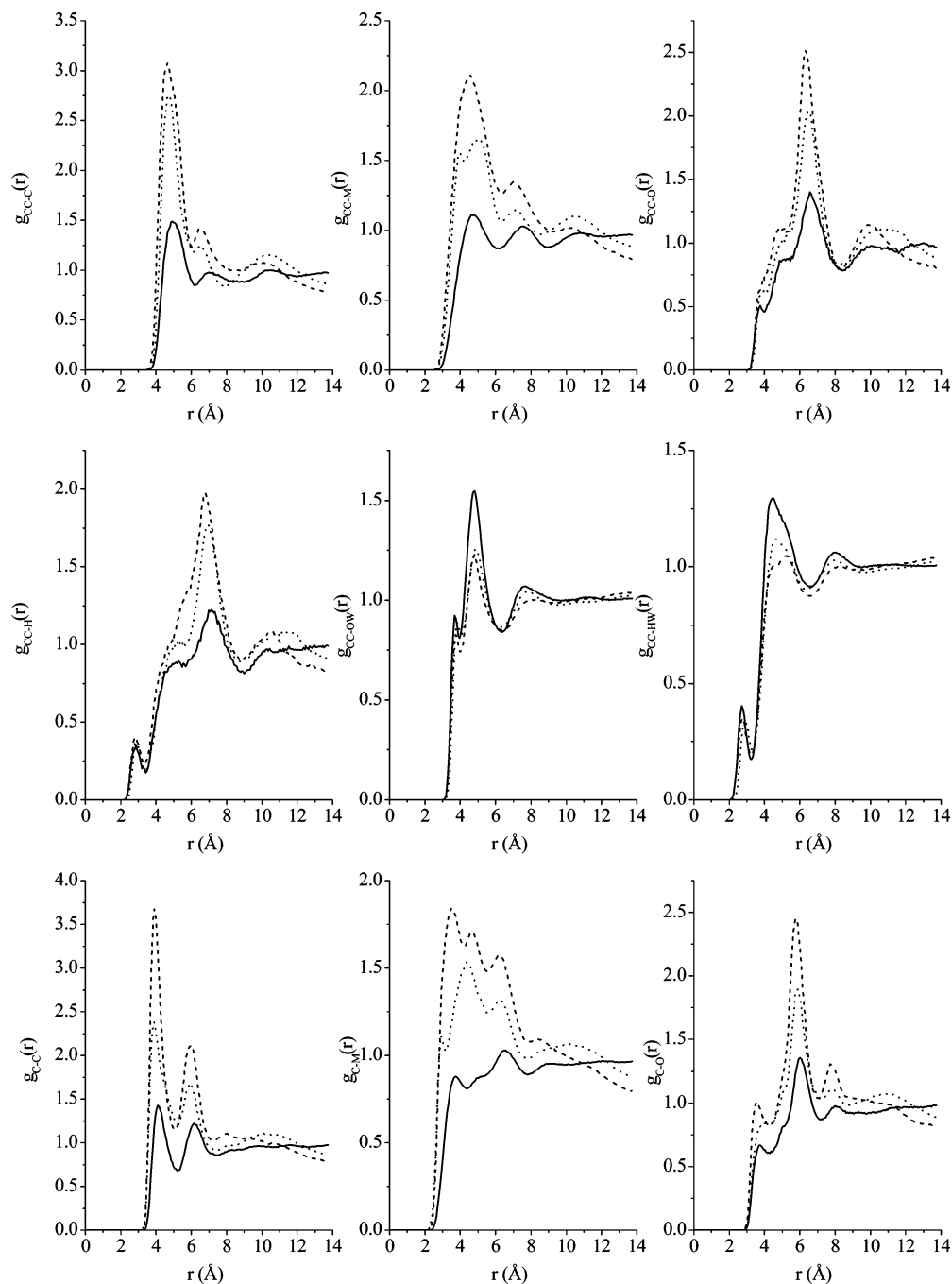


Figure 4. Partial pair distribution functions for CC–C, CC–M, CC–O, CC–H, CC–OW, CC–HW, C–C, C–M, and C–O derived from the EPSR models at (—) 25, (---) 80, and (···) 106 °C.

coordination number to 2.4; this parallels the (small but significant) fall in the small-angle neutron scattering (Figure 1).

Changes in the solute–solute structure must be accompanied by changes in the solute–solvent structure, and these can be assessed through the central carbon–water oxygen partial radial distribution function shown in Figure 4. The first peak of this function has a small feature centered at a distance of about 3.5 Å, which relates to water molecules hydrogen-bonded to the polar tail of the alcohol. The larger feature centered at about 5 Å relates to the water molecules in contact with the head group region; the reduction in this peak as the temperature rises to 80 °C reflects a reduction (of about 20% in terms of coordination number; see Table 2) in the average number of water contacts in the head group region. With further temperature increase,

this peak increases a little, suggesting the head group hydration has begun to increase again by 106 °C.

Before beginning to look at the details of the nature of the interactions that might be occurring between the solute and solvent molecules as temperature increases, we should pause to consider changes that may be occurring at larger distances from a central solute molecule. We have already noted that, in passing through the SANS maximum, there is a change in the medium-range clustering (see Figures 3 and 8), and such changes must reflect changes in relevant partial radial distribution functions beyond the first-neighbor peaks; we are trying to understand what the local structural data are telling us about the nature of medium-range structures, and so the nature of the intermolecular contacts at longer than first-neighbor distances should be examined.

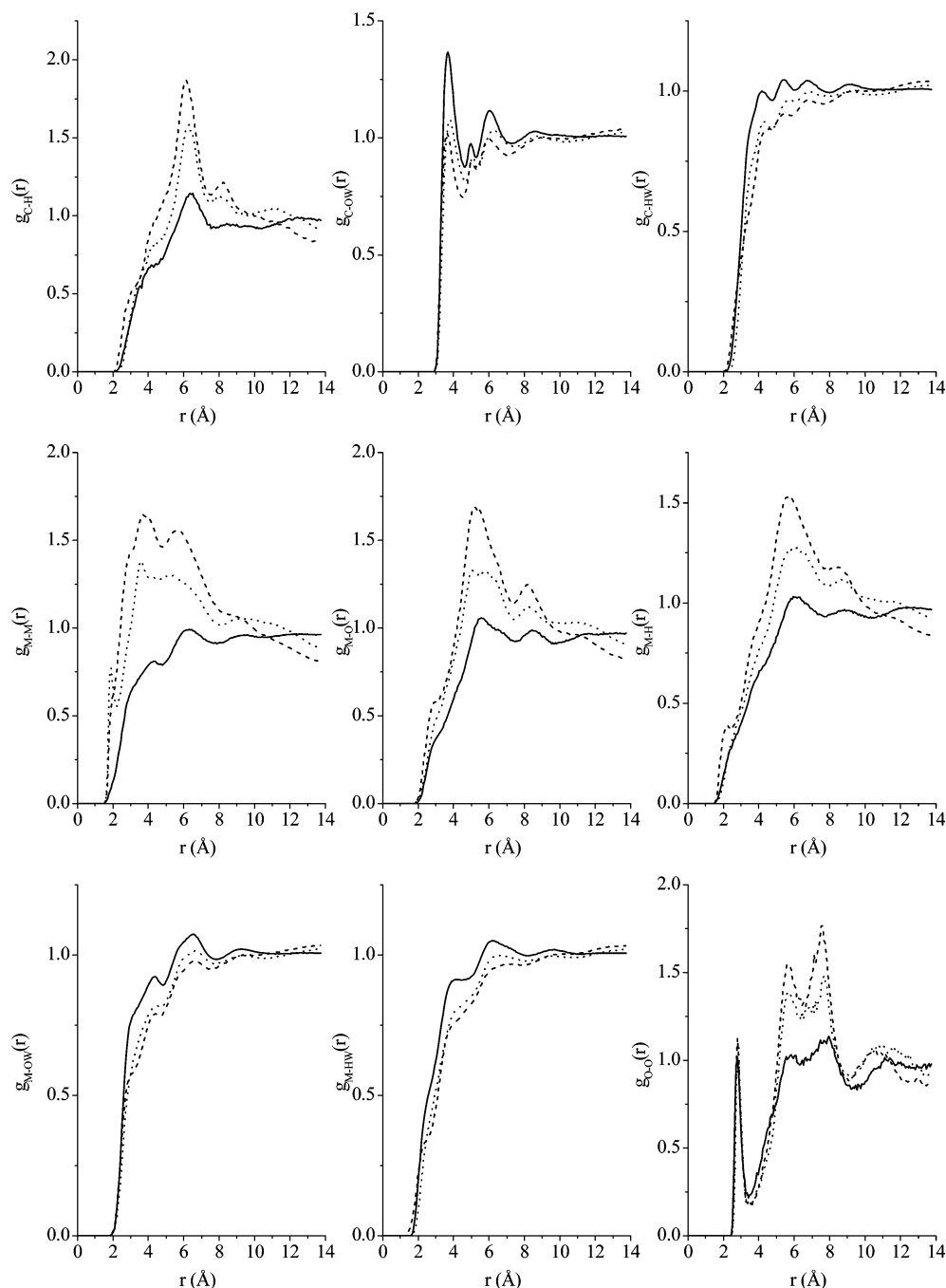


Figure 5. Partial pair distribution functions for C–H, C–OW, C–HW, M–M, M–O, M–H, M–OW, M–HW, and O–O derived from the EPSR models at (—) 25, (---) 80, and (···) 106 °C.

First, in the solute–solute distribution function of Figure 7, the second peak at about 9–10 Å significantly increases between 25 and 80 °C; this is consistent with what we have observed earlier concerning the increase in larger clusters with temperature. With a further increase in temperature to 106 °C, the main effect observed in this second-neighbor region is an outward shift in the peak position by about 1 Å, indicating a moving out of second neighbors that could be consistent with beginning of breakdown of the larger clusters. Second, referring to the second-neighbor region of the *tert*-butanol–water (CC–OW) function between 7 and 8 Å (Figure 4), we see a significant drop in size when the temperature is raised from 25 to 80 °C, presumably relating to displacement of water by solute molecules as larger solute clusters are formed. Increasing the temperature further to 106 °C shows some recovery in this peak,

suggesting additional waters are involved in the breaking down of the larger clusters found in the 80 °C data.

More light can be shed on the detailed nature of the temperature-dependent clustering by referring to the *tert*-butanol–water spatial density function (SDF) sections of Figure 12 and the full SDFs of Figure 13. In Figure 12, the bright features at about 5 and 7 o'clock relate to the water molecules hydrogen-bonding to the polar groups of the alcohol molecules; there is no major change in the intensities of these lobes at the different temperatures. Referring to the equivalent full SDFs in the top line of Figure 13 does suggest some small changes, however, in that the three water lobes are more distinct from each other at 25 and 106 °C than they are at the intermediate temperature, perhaps implying slightly less water localization at 80 °C.

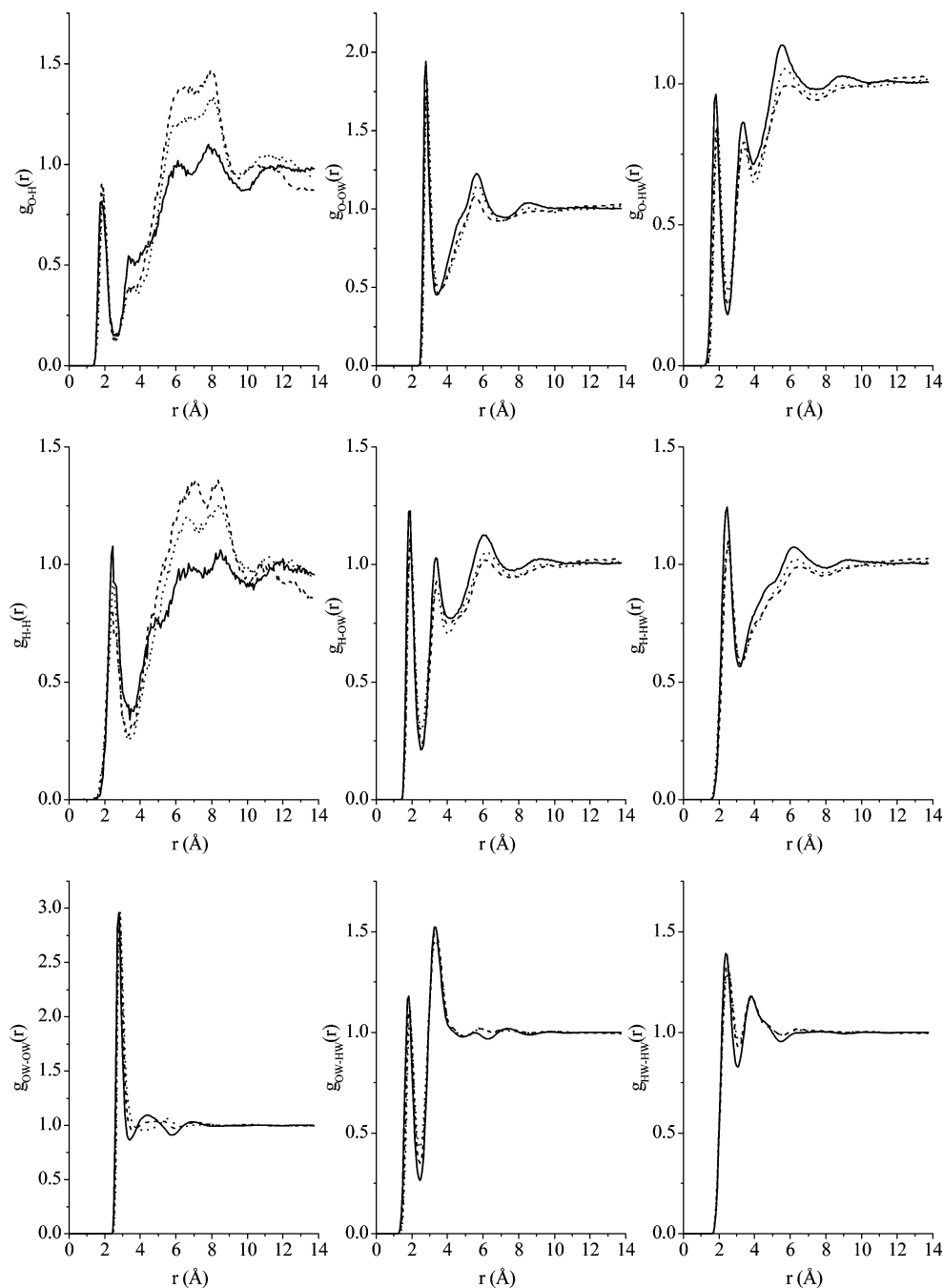


Figure 6. Partial pair distribution functions for O–H, O–OW, O–HW, H–H, H–OW, H–HW, OW–OW, OW–HW, and HW–HW derived from the EPSR models at (—) 25, (---) 80, and (···) 106 °C.

The lobes at the sides and top of the maps in Figure 12, which relate to the water molecules adjacent to the nonpolar parts of the *tert*-butanol molecule, show significant changes with temperature. Considering first the lobe centered at 12 o'clock at 25 °C (Figure 12a), this largely falls away at 80 °C and then begins to grow back at 106 °C. Similarly, the lobes at the sides of the molecule reduce in intensity as temperature increases, though perhaps there is some slight recovery at 106 °C. Overall, these maps indicate that as the temperature rises to 80 °C, water is being excluded from the region at the top and around the sides of the nonpolar region of the *tert*-butanol molecule, presumably being displaced by other solute molecules; the slight recovery at 106 °C implies that water is beginning to seep back into these regions.

There is one further interesting temperature-related change in Figure 12 that needs to be remarked upon. This concerns the

broad halo at a distance of about 8 Å that can be seen in the corner regions of the correlation maps in the distance range beyond 7.5 Å and that forms an extended ring if plotted on a larger scale. This relates to the second-neighbor peak in the CC–OW partial (Figure 4) that we commented on above. As we increase the temperature to 80 °C, this halo fades, most noticeably in the upper half of the figure. At the highest 106 °C temperature, the halo begins to return as the equivalent peak in the CC–OW partial RDF increases. In addition to concluding that the nonpolar head at the first-neighbor level loses significant water at 80 °C but regains some of it at 106 °C, similarly, at the second-neighbor level, the nonpolar region loses nearly all its water at 80 °C but regains some of it at 106 °C.

These interpretations are strengthened by considering the full *tert*-butanol–water spatial density functions in the second and third rows of Figure 13. The second row of this figure presents

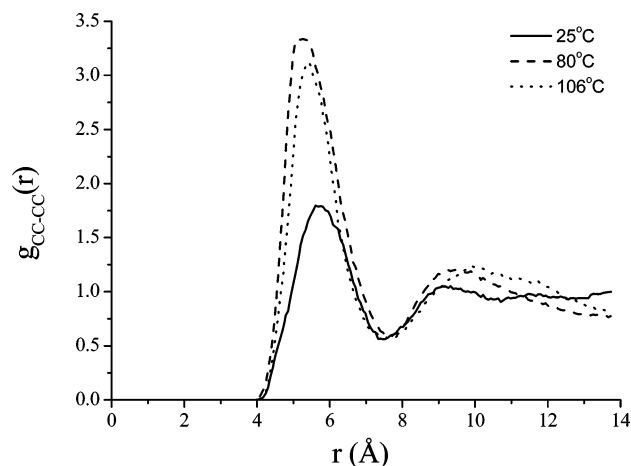


Figure 7. *tert*-butanol–*tert*-butanol molecular centers pair distribution function CC–CC derived from the EPSR models at (—) 25, (---) 80, and (···) 106 °C.

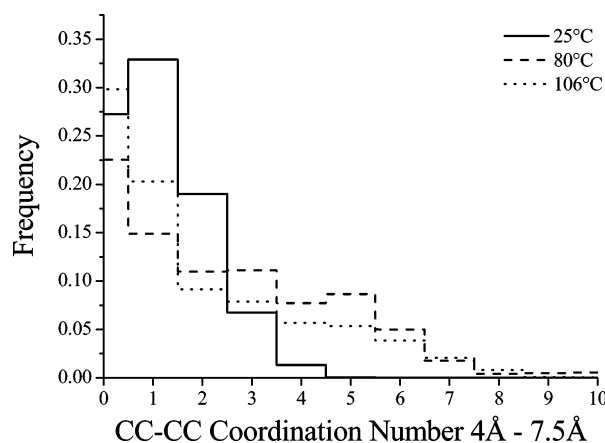


Figure 8. Coordination number histogram for *tert*-butanol molecules around *tert*-butanol molecules in the distance range from 4 to 7.5 Å, illustrating the growth and decrease in larger cluster sizes as the temperature is increased from (—) 25 to (---) 80 to (···) 106 °C.

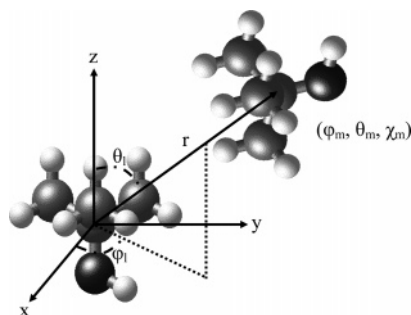


Figure 9. Coordinate reference frame illustrating the angles used in the EPSR calculation of the orientational correlation functions for *tert*-butanol interactions. The variables θ_1 and ϕ_1 are referenced to a *tert*-butanol molecule placed at the origin, while ϕ_m , θ_m and χ_m correspond to the angular orientation of a neighboring *tert*-butanol molecule found at a distance r from the origin.

the distribution of first-neighbor waters around a central *tert*-butanol; this shows a reduction as the temperature rises from 25 to 80 °C (note the “holes” in the contour above the *tert*-butanol molecule), followed by a subsequent increase at 106 °C. As the only other component that is present in the system is *tert*-butanol, this implies that the water is being increasingly excluded from the nonpolar head group at 80 °C by the presence of other solute molecules. The enhanced clustering at this temperature therefore is consistent with increasing nonpolar–

nonpolar contacts already observed and commented on above. As we move to the higher 106 °C temperature, where SANS has already told us that the clustering is beginning to break up, water increases its presence in the nonpolar head group region, presumably as the *tert*-butanol neighbors begin to fall away as the clustering begins to break down. During these temperature increases, however, we note that the waters at the polar end are little perturbed (see Figure 13a–c), though as already indicated there may be small changes such as the slight delocalization of polar waters at the intermediate 80 °C temperature (Figure 13b) and possibly a small drop in the *tert*-butanol–water hydrogen-bonded coordination number (see the O–OW coordination number in Table 2). These changes at the polar end of the solute molecule are, however, relatively small: whatever the local geometry of the clustering molecules is, it must be accommodated with the polar ends of the *tert*-butanol molecules making hydrogen bonds to water rather than to other alcohol molecules. This is similar to the way in which a real micellar system is expected to interact with water, with the polar ends of the amphiphile molecules hydrogen-bonding to the surrounding solvent.

The changes in the second-neighbor region (line 3 of Figure 13) as we raise the temperature are quite dramatic. At 25 °C, the head group region is surrounded by waters, consistent with the small solute cluster size at this temperature (cf. the structure snapshots shown in Figure 3). Increasing the temperature to 80 °C completely denudes this region of solvent: the solute clustering has displaced most of the water in this second-neighbor shell. Increasing the temperature further to 106 °C shows the water beginning to move back around the side of the molecule into this region as the average cluster size begins to fall, though there is still significant water exclusion in the top part of the head group region.

Although these results give us a good qualitative picture of what is happening at the molecular level as the *tert*-butanol molecules first cluster and then begin to disassemble as we go over the SANS maximum, there are further data that we can interrogate to try to obtain a semiquantitative geometrical picture of the assemblies of *tert*-butanol molecules. Although it must be remembered that we are looking at a liquid, and that therefore any picture we try to draw of these aggregates must of necessity be an average one, such a picture might help us to begin to understand the nature of the intermolecular interactions occurring in these assemblies and hence perhaps driving, or modulating, the self-assembly process. To try to throw light on these *tert*-butanol aggregates, we look at the *tert*-butanol–*tert*-butanol SDFs with the initial intention of assessing how the solute molecules fill in the region that has been vacated by the water around the nonpolar regions.

We have already noted that the 25 °C *tert*-butanol–*tert*-butanol orientational correlation function of Figure 11 indicates a near 90° relative orientation of *tert*-butanol molecules, as indicated schematically by the cartoon on the left of Figure 11. This orientation relates to the 9–10 o'clock lobe in the orientational correlation function plot in this figure. The feature between 3 and 4 o'clock indicates also a population of –90° mutual orientations; its lower intensity relates to the need to accommodate the 3-fold symmetry of the molecule's head group. As the average solute–solute coordination number is only 1.8, we can consider these mutual orientations to be the dominant ones in the small clusters at this lowest temperature.

Figure 14 shows the temperature-induced changes in the appropriate solute–solute SDF maps. Upon going from 25 to 80 °C—the maximum in the clustering—there is a clear intensity

TABLE 2: Coordination Numbers for a 0.04 Mole Fraction Solution of *tert*-Butanol in Water at 25, 80, and 106 °C

| correlation | density (atoms Å ⁻³) | R_{\min} (Å) | R_{\max} (Å) | atoms ^a | | |
|-------------|----------------------------------|----------------|----------------|--------------------|-------------|-------------|
| | | | | 25 °C | 80 °C | 106 °C |
| CC–CC | 0.0011 | 4.0 | 7.5 | 1.8 ± 0.4 | 2.8 ± 0.6 | 2.4 ± 0.5 |
| | | 4.0 | 6.0 | 0.8 ± 0.3 | 1.6 ± 0.4 | 1.4 ± 0.4 |
| OW–OW | 0.0276 | 2.5 | 3.4 | 4.1 ± 0.1 | 4.4 ± 0.1 | 4.5 ± 0.1 |
| | | 3.4 | 5.8 | 22.1 ± 0.3 | 18.2 ± 0.3 | 18.0 ± 0.3 |
| CC–OW | 0.0276 | 3.0 | 4.0 | 2.3 ± 0.3 | 2.1 ± 0.3 | 2.0 ± 0.3 |
| | | 4.0 | 6.5 | 26.0 ± 1.0 | 23.0 ± 1.3 | 23.8 ± 1.3 |
| CC–HW | 0.0552 | 2.0 | 3.2 | 1.3 ± 0.2 | 1.2 ± 0.2 | 1.0 ± 0.2 |
| | | 3.2 | 6.5 | 55.9 ± 1.5 | 49.3 ± 2.3 | 50.8 ± 2.2 |
| O–O | 0.0011 | 2.3 | 3.5 | 0.1 ± 0.1 | 0.1 ± 0.1 | 0.1 ± 0.1 |
| | | 3.5 | 8.5 | 2.5 ± 0.4 | 3.3 ± 0.6 | 3.0 ± 0.5 |
| O–H | 0.0011 | 1.4 | 2.6 | 0.03 ± 0.03 | 0.03 ± 0.03 | 0.03 ± 0.03 |
| | | 2.6 | 9.0 | 3.0 ± 0.3 | 3.9 ± 0.4 | 3.6 ± 0.4 |
| O–OW | 0.0276 | 2.5 | 3.5 | 2.8 ± 0.3 | 2.7 ± 0.3 | 2.8 ± 0.3 |
| | | 3.5 | 7.0 | 34.7 ± 1.2 | 31.7 ± 1.4 | 32.4 ± 1.4 |
| O–HW | 0.0552 | 1.3 | 2.5 | 1.4 ± 0.2 | 1.3 ± 0.2 | 1.3 ± 0.2 |
| | | 2.5 | 4.0 | 7.6 ± 0.5 | 7.1 ± 0.6 | 7.1 ± 0.6 |
| H–OW | 0.0276 | 1.4 | 2.6 | 0.9 ± 0.2 | 0.9 ± 0.2 | 0.9 ± 0.2 |
| | | 2.6 | 4.5 | 6.5 ± 0.5 | 6.1 ± 0.5 | 6.0 ± 0.5 |
| H–HW | 0.0552 | 1.7 | 3.3 | 5.3 ± 0.5 | 5.0 ± 0.5 | 5.2 ± 0.5 |
| OW–HW | 0.0552 | 1.3 | 2.5 | 1.7 ± 0.1 | 1.8 ± 0.1 | 1.8 ± 0.1 |
| | | 2.5 | 4.6 | 20.7 ± 0.2 | 21.1 ± 0.2 | 21.1 ± 0.2 |
| HW–HW | 0.0552 | 1.6 | 3.0 | 5.0 ± 0.1 | 5.2 ± 0.1 | 5.2 ± 0.1 |

^a Note that the range quoted is an indication of the range of coordination numbers found in the ensembles; it is not a standard error.

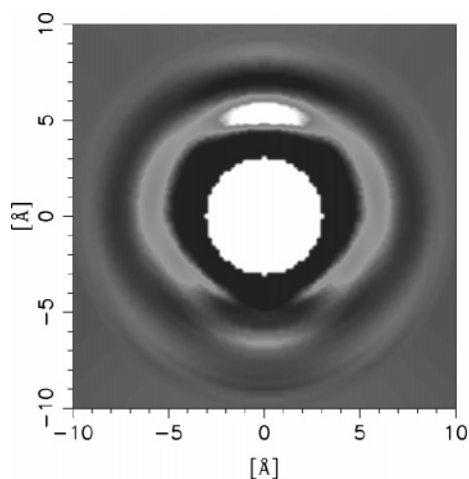


Figure 10. Spatial density map, averaged over φ_1 , showing the relative probability of finding the central carbon atom (CC) of a neighboring *tert*-butanol molecule around any arbitrarily selected *tert*-butanol molecule placed at the origin and oriented with its nonpolar methyl groups toward the top of the figure, calculated for a 0.04 mole fraction solution of *tert*-butanol in water at 25 °C.

increase in the 12 o'clock lobe relating to the head-to-head contacts, together with a significant increase in the 2 and 10 o'clock regions relating to contacts further down the sides of the solute molecule (compare Figure 14a with Figure 10). As the clustering begins to fall off at 106 °C (see Figure 14b), the 12 o'clock intensity falls a little, while the lobes at 2 and 10 o'clock also lessen. The initial indication is that the nonpolar–nonpolar contacts increase at 80 °C, including contacts at the side of the molecule as well as at the tops, and with further temperature increase, both these contacts begin to reduce.

To explore the nature of the solute–solute contacts in the larger clusters at 80 °C, we refer to the θ_m map for $\theta_1 = 0$ in Figure 15a. Both the left- and right-hand lobes relating to the $\pm 90^\circ$ relative orientations increase in intensity compared to 25 °C (cf. Figure 11), indicating an unsurprising increased population of these T-like orientations as the average cluster size increases. In addition, there is a significant feature at 6 o'clock that indicates a significant population of the head-to-head 180°

relative orientation that dominates at the 25 °C 0.02 and 0.06 mole fraction concentrations, as mentioned earlier. A further interesting point arises relating to the increase in the 9–10 Å second-neighbor peak in the RDF of Figure 7: the lower lobe at 6 o'clock in the SDF of Figure 15a shows that the molecular orientations relating to this peak are also head-to-head 180° ones, but with a difference: the head groups are not in contact but are not quite far enough apart to accommodate an intervening head group directly in between them. One possibility might be intervening water; however, investigation of the relevant *tert*-butanol–water SDF (Figure 12b) shows relatively little water in this region. We might tentatively suggest that the intervening space is filled by other *tert*-butanol molecules squeezed out slightly to the sides (cf. discussion below). This is, interestingly, a frequently found local structure in noncrystalline systems whose structures are dominated by packing forces.^{24,25}

Other orientations of dimers are indicated by the (strong) $\pm 55^\circ$ and (weaker) $\pm 110^\circ$ lobes in the 80 °C plot of Figure 14. The details of these orientational configurations for the three temperatures can be seen in Figure 16. The configurations associated with the $\pm 110^\circ$ lobes bring parts of neighboring *tert*-butanol molecules toward the polar end of the central molecule, an approach that could encourage the decreased localization of the tail-interacting waters at this temperature suggested earlier (cf. Figure 13b).

Moving now to 106 °C, Figure 15b shows lobes corresponding to 90° (T-like) and 180° (in-line) relative orientations. There are significant differences in the relative lobe intensities compared to 80 °C (Figure 15a): the 90° T-like populations appear to fall relative to a rise in the 180° in-line population. Moreover, several of the alternative populations of the kind indicated for the 80 °C case are reduced, as indicated by the lower intensities of the corresponding lobe regions in Figure 15b. The separated second-neighbor populations indicated in the bottom 6 o'clock lobe of Figure 15a for 80 °C are also reduced by becoming more diffuse and less localized. We have already observed that the “separated” structure indicated in Figure 15a is consistent with characteristic structures found in simple sphere packings.^{24,25} This increased diffuseness of the corresponding feature in the relevant orientational pair correla-

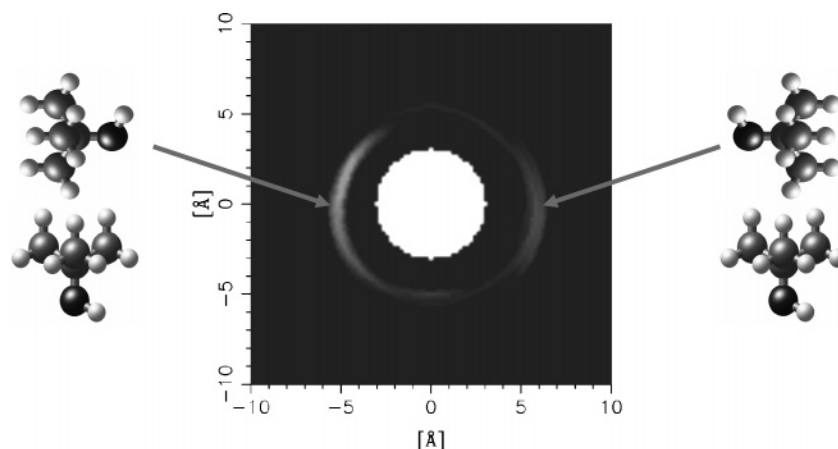


Figure 11. Orientational correlation map calculated as a function of θ_m for $\varphi_1 = \theta_1 = \varphi_m = \chi_m = 0^\circ$ and showing the preferred orientations of a neighboring *tert*-butanol molecule that would be located in the bright “12 o'clock” lobe centered at (0,5) in Figure 10.

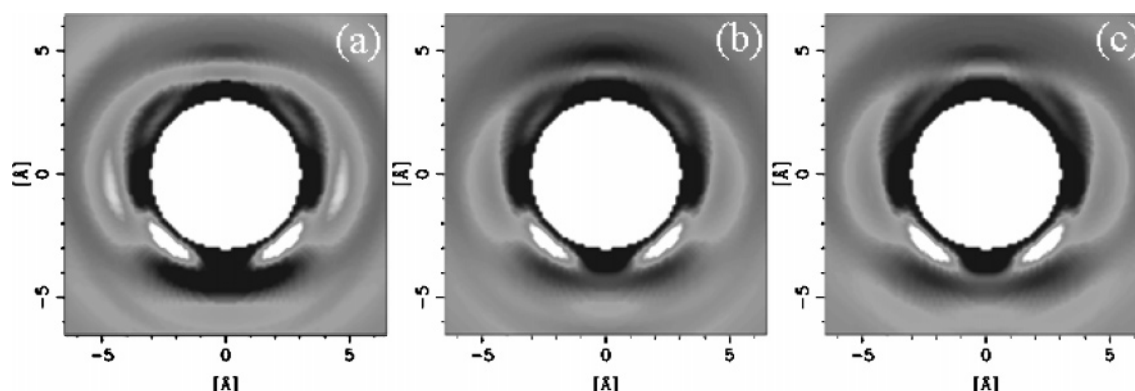


Figure 12. Spatial density maps, averaged over φ_1 , showing the relative probability of finding a water oxygen atom (OW) of a neighboring solvent molecule around any arbitrarily selected *tert*-butanol molecule placed at the origin and oriented with its nonpolar methyl groups pointing toward the top of the figure. The maps are calculated for a 0.04 mole fraction solution of *tert*-butanol in water at (a) 25, (b) 80, and (c) 106 °C. In all three figures the two bright lobes in the lower half of the figure correspond to water molecules hydrogen-bonding to the hydroxyl group of the alcohol molecule.

tion function map seems to be consistent with a reduction in the effects of packing constraints within the aggregating solute units as the structures found at 80 °C begin to lose their structural integrity.

These results build up a picture in which a simple average $\sim 90^\circ$ T-like dimer is the basic average local arrangement in the small solute clusters observed at 25 °C. At the SANS maximum at 80 °C, where the cluster size is greatest, the population of these relative orientations increases; a number of other relative nonpolar–nonpolar contact orientations also come into play, including a significant population of head-to-head separated configurations (Figure 15a). For this maximally clustered system, the solute–water SDFs indicate that the water is largely excluded from the top of the head group region in the near-neighbor region and strongly excluded at what might be termed second-neighbor distances (Figure 13h).

Increasing the temperature to 106 °C results in a reduction in complexity of local relative orientations as the clusters begin to break up. There is an interesting switch between the relative populations of T-like and in-line configurations, the latter increasing and the former decreasing. There is also increased penetration of water around the nonpolar head (Figures 12c and 13f); in the second-neighbor distance region, this ingress of water is particularly evident around the sides of the head group in the side regions as indicated in Figure 13i. Thus, the breakdown of clusters with increasing temperature is not simply a reversal of the clustering process: we seem to be moving to a different kind of structure that reflects a different resolution

of the competition between the different kinds of interactions (hydrogen bonding and nonpolar–nonpolar interactions), presumably as a consequence of their different temperature dependencies.

It is perhaps of interest finally to look at the kinds of dimers that the data indicate are present in the large clusters at 80 °C and consider how the kinds of mutual solute arrangements identified in the orientational correlation maps might be fitted together to form a plausible cluster that is also consistent with the need for the polar tails of the molecules to—as in a micellar structure—interact directly with the solvent. This is of course a three-dimensional problem, but a two-dimensional analogue can give some insight to the kind of possible structures that might be obtained. Such a one is shown in Figure 17, which is broadly consistent with the local pair orientations identified from the orientational distribution maps yet in which the requirement to hydrogen-bond to solvent is also fulfilled. One particular point worth noting is the mutual coexistence of the separated head-to-head arrangement (molecules A and B in Figure 15) with the contact T-like orientation.

A full description of the local arrangements in the structure can be examined further by other techniques such as Voronoi polyhedron analyses.^{24–26} From the present analysis, however, we can take away perhaps two messages. First, the kinds of clusters that can be built of *tert*-butanol molecules consistent with observed local orientations are overall consistent with the kinds of local geometries observed in simpler packed sphere structures; the combination of contact and separated head-to-

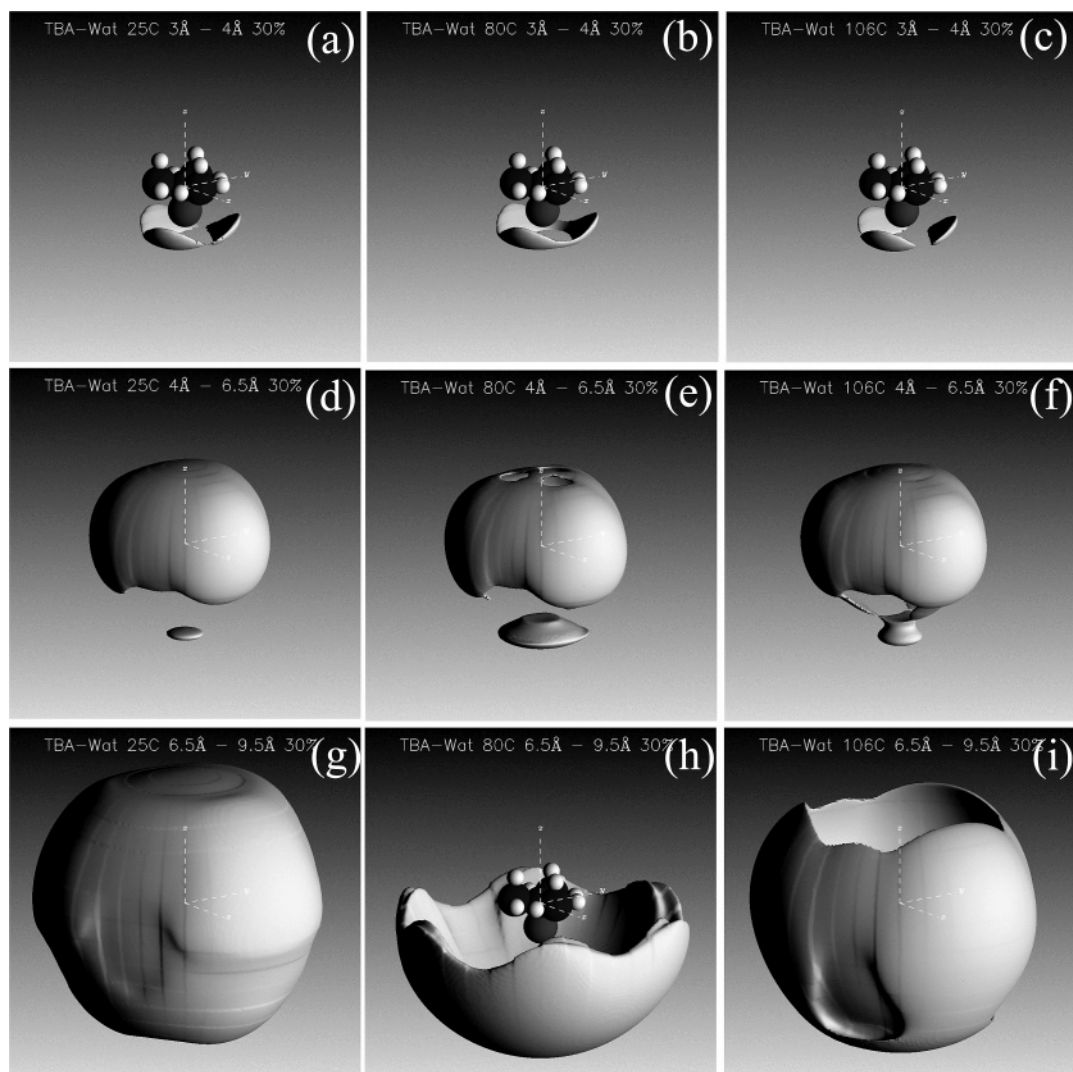


Figure 13. Three-dimensional spatial density functions showing the preferred hydration regions of *tert*-butanol molecules in a 0.04 mole fraction solution as a function of temperature and radial distance. The density surfaces correspond to the 30% most favorable probability regions of finding a solvent water oxygen atom around a *tert*-butanol molecule placed at the origin. (a, d, g) 25 °C; (b, e, h) 80 °C; (c, f, i) 106 °C. The radial shells highlighted in the figures correspond to distances 3–4 Å from the central carbon atom sited on the origin for panels a–c, 4–6 Å from the origin for panels d–f, and 6.5–9.5 Å for panels g–i, highlighting in turn the hydrogen-bonding regions between solute alcohol and solvent water, the nonpolar hydration shell of the alcohol molecules, and the second-neighbor hydration shell of the alcohol molecules.

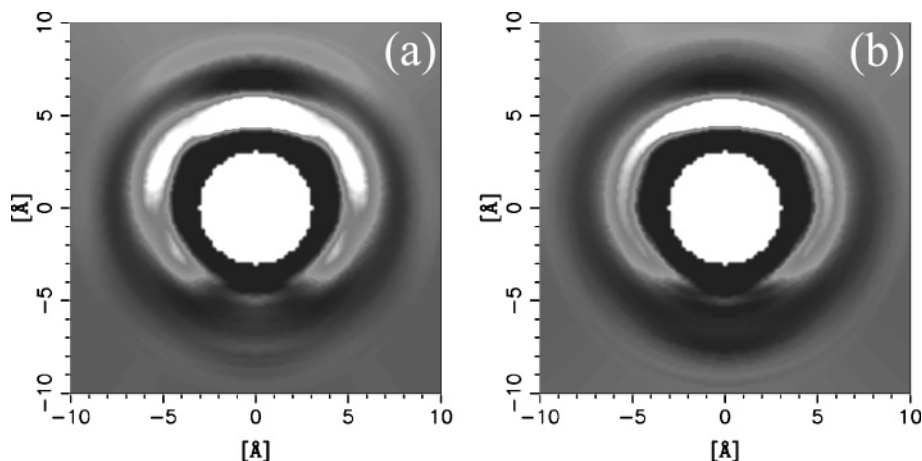


Figure 14. Spatial density maps, averaged over φ_1 , showing the relative probability of finding the central carbon atom (CC) of a neighboring *tert*-butanol molecule around an arbitrarily selected *tert*-butanol molecule placed at the origin and oriented with its nonpolar methyl groups pointing toward the top of the figure, calculated for a 0.04 mole fraction solution of *tert*-butanol in water at (a) 80 and (b) 106 °C.

head structures observed here are very reminiscent of the main local structures observed in hard-sphere packings used to model ideal liquids.^{24,25} Second, they are also consistent with the

dominant interaction of the alcohol tail being with water rather than other alcohol molecules. Thus the kinds of structures that appear to be indicated by the experimental data represent ones

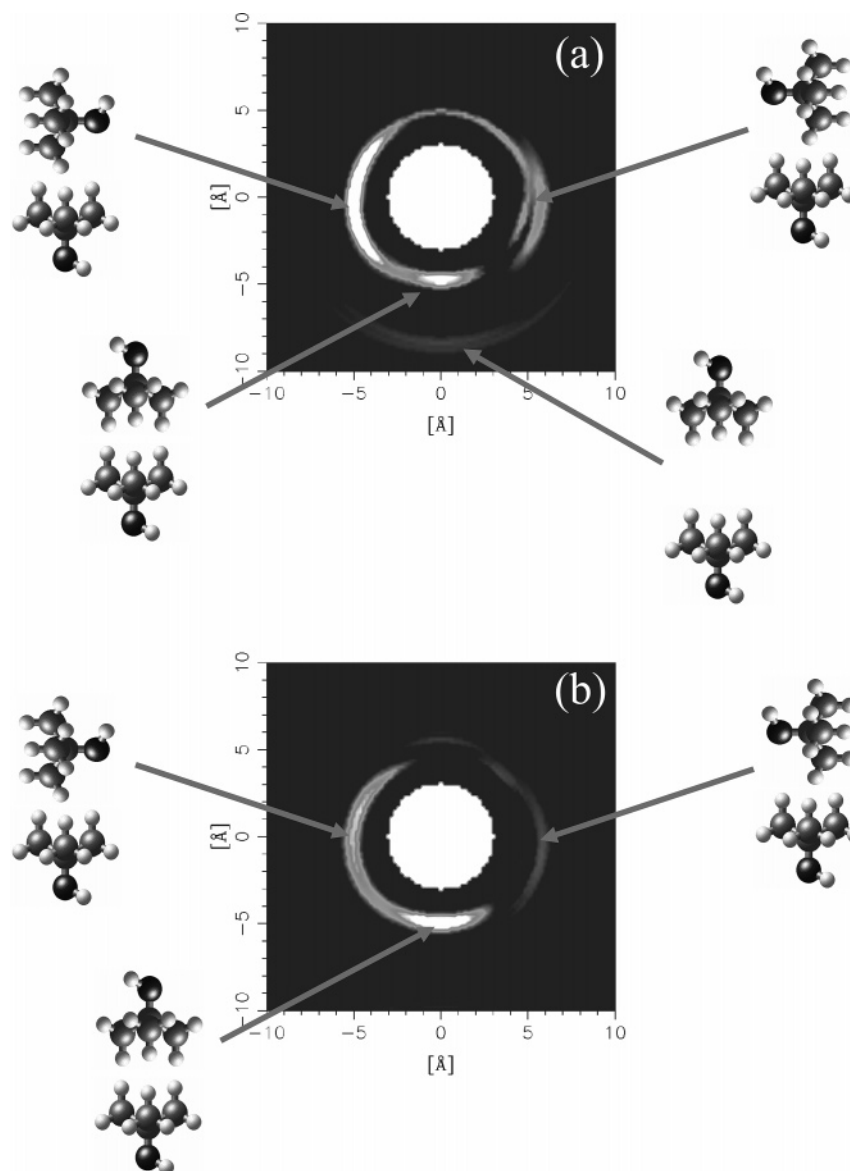


Figure 15. Orientational correlation maps calculated as a function of θ_m for $\varphi_l = \theta_l = \varphi_m = \chi_m = 0^\circ$ and showing the preferred orientations of a neighboring *tert*-butanol molecule that would be located in the bright lobes centered at (0,5) in Figure 14 for the solutions at (a) 80 and (b) 106 °C. Illustrations of the principal molecular configurations are included for clarity.

that are consistent with a simple packed structure of nonpolar head groups but that also satisfy the hydrogen-bonding demands of the polar tail and the solvent water.

Conclusions

One of the reasons for looking at the temperature-dependent molecular-level structure of the *tert*-butanol system was to try to understand at the molecular level the kinds of interactions that occur as the clustering increases and then decreases as the temperature is raised. It seems to be generally accepted that the hydrophobic interaction increases with increasing temperature up to a maximum, and then falls off: hence the clustering behavior observed as the temperature of an appropriate aqueous solution is increased is generally rationalized as a manifestation of the hydrophobic interaction. Experimental evidence does exist for a minimum in solubility of nonpolar molecules in water, which would be consistent with this hypothesis.^{1–3} Moreover, small-angle scattering data on amphiphiles also implies first a rise and then a fall in clustering as the system goes through a maximum.¹¹

The results of neutron scattering with isotopic substitution have enabled us to see the kinds of local interactions that occur both within the solute clusters and between the solute and solvent as the solute molecules assemble into clusters and then begin to break down with further increase in temperature. As would indeed be expected for a system whose behavior is dominated by the hydrophobic interaction, the clusters observed in the maximally aggregated system do show extensive contact between nonpolar head groups of interacting molecules. Looking at pairs of interacting *tert*-butanol molecules, however, there are some quite subtle changes in the relative populations of particular dimer configurations as we go through the temperature maximum. Moreover, considering the changes in these relative populations, the cluster breakdown does not seem to be a simple reversal of the assembly process.

One interesting aspect of this nonreversibility in detailed structure relates to the dominant solute–solute interaction geometry. At room temperature, this is a 90° T-like mutual arrangement—interestingly contrasting with the in-line 180° that has been observed to dominate at other concentrations.^{13–16} As

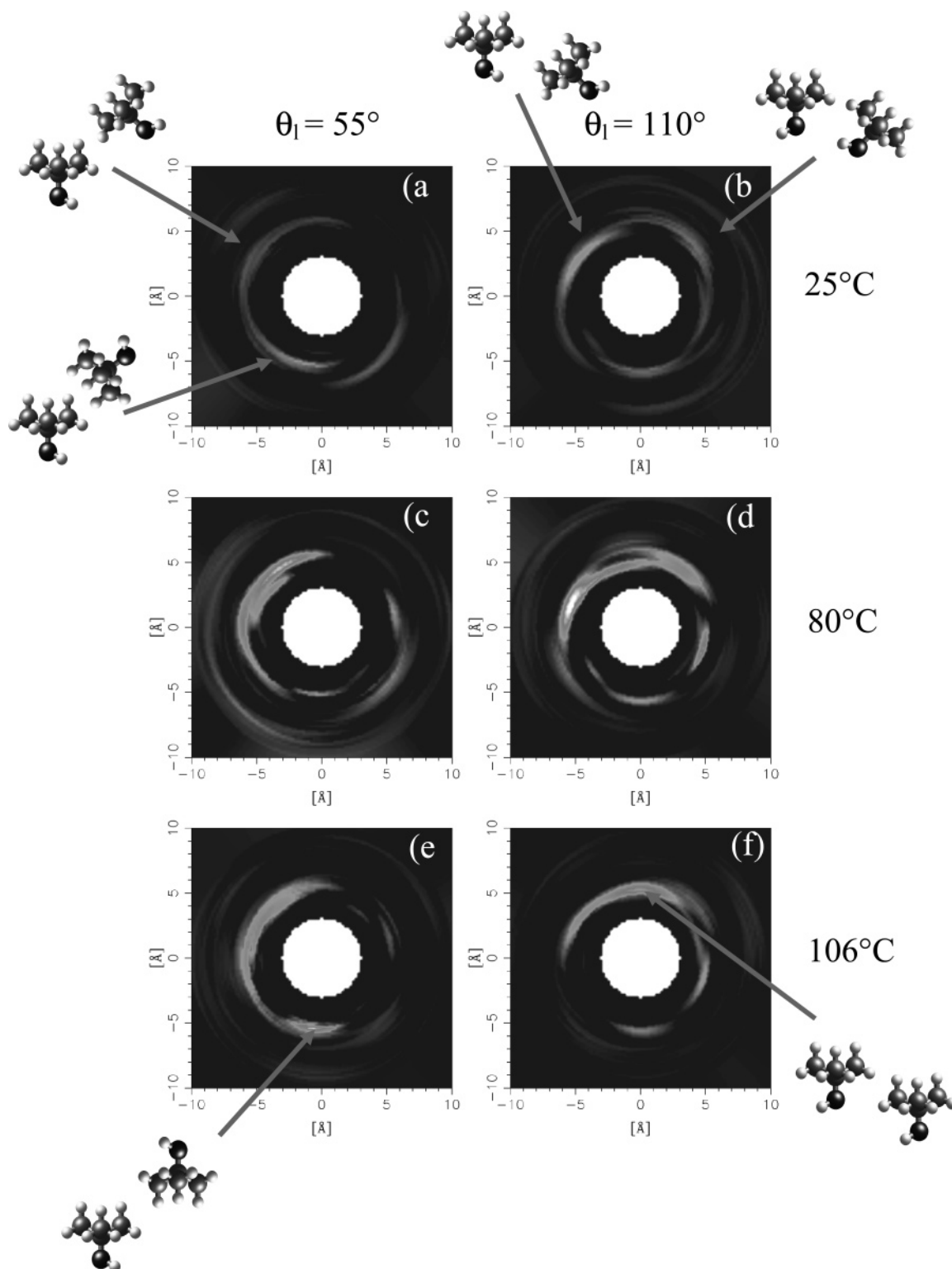


Figure 16. Orientational correlation maps of *tert*-butanol relative to *tert*-butanol calculated as a function of θ_m for (a, c, e) $\varphi_l = \varphi_m = \chi_m = 0^\circ$ and $\theta_l = 55^\circ$ and for (b, d, f) $\varphi_l = \varphi_m = \chi_m = 0^\circ$ and $\theta_l = 110^\circ$. Solution of *tert*-butanol, 0.04 mole fraction, at (a, b) 25, (c, d) 80, and (e, f) 106 °C were used. Also illustrated are the preferred orientations highlighted by a selection of the features in the orientational correlation maps.

temperature increases, these T-like mutual configurations are joined by a number of others, one of which is the in-line structure. Throughout this assembly process, the polar tail end of the alcohol continues to be dominated by hydrogen bonding to solvent water, with no indication of significant solute–solute interaction via direct hydrogen-bonding interactions between alcohol tail groups. Water is increasingly excluded from the head group region as the temperature maximum is approached, and it is possible to build up, from the observed frequently

occurring mutual arrangements of solutes, structures for the maximal clusters that fulfill packing constraints between head groups yet also allow near-maximal interaction of the polar tails with water in a sort of close-packed micellar kind of arrangement.

As temperature increases further, beyond that at which the small-angle neutron scattering is a maximum, water begins to leak back around the nonpolar head groups and the clusters begin to break up. Interestingly, the breakup is not the reverse

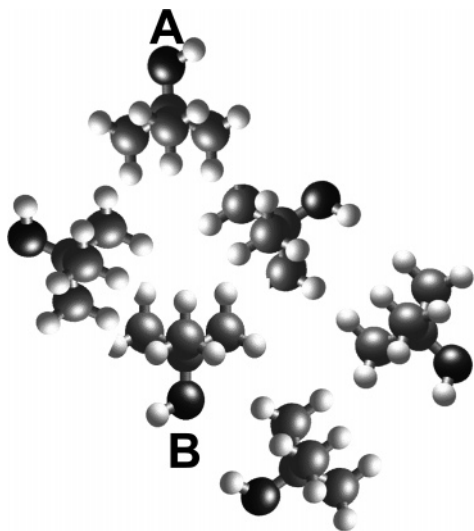


Figure 17. Two-dimensional conceptual diagram of a cluster of *tert*-butanol molecules involving typical alcohol–alcohol interactions that appear consistent with the EPSR model evaluated from the experimental data.

of the assembly process. Perhaps most notable is the change in relative populations of the T-like and in-line mutual arrangements. As we pass over the maximum, the structure does not revert to one dominated by the T-like configuration. Rather, the population of the 180° in-line arrangement grows. In terms of the local solute–solute arrangements, therefore, the high-temperature 0.04 mole fraction solution bears a closer resemblance in this characteristic to the room-temperature 0.02 and 0.06 concentration solutions than it does to its own room-temperature structure.

The possible 80 °C cluster structures that can be built up consistent with the orientational information obtained from the neutron measurements mirror the kinds of structures seen in systems where packing constraints dominate. Additionally, however, the amphiphile–water system needs to satisfy the hydrogen-bonding constraints of the polar tail, and these postulated structures can be constructed to satisfy these additional constraints. Interestingly, the packing constraints within the body of the micelle may constrain a little the hydrogen bonding in the polar tail region: as water is expelled from the nonpolar regions of the solute, more waters need to be accommodated at the tails, and the geometrical restrictions there may result in some slightly increased but significant disordering of the hydrogen-bonding geometry. As the micelles begin to break up, these constraints are relaxed and the hydrogen-bonding region looks less strained.

Although the clustering observed may qualitatively appear to be consistent with being driven by hydrophobic interactions, the effects we observe at the molecular level imply a rather more complex interplay between the nonpolar and polar interactions operational in the system. It may well be that the solubility variation with temperature of inert gases indeed does reflect the variation in the hydrophobic interaction as such, but in the case of amphiphiles, which are the kinds of molecules relevant to those systems in which the importance of hydrophobic interactions is often emphasized (protein folding and stability, micelle formation, etc.), the importance of polar interactions in such structures cannot be ignored. The relevance of the polar interactions has been argued previously in related work in several systems.^{14–16,21} How a particular system resolves the competing interactions is not at present explainable in a simple way even for a single system at a single temperature;

once we look at concentration, temperature, and pressure variation, the different variabilities of the different competing interactions will complicate the situation even further, and it becomes increasingly difficult to predict how the particular system will resolve this competition. What perhaps might be argued, however, is that it is likely to be a mistake to oversimplify a process in terms of the dominance of a particular kind of interaction. In the case of amphiphiles in water, it is becoming increasingly difficult to see how the effects of a hydrophobic driving force can be separated from the effects of the polar interactions involved in the system.

From a range of studies, we are seeing increasingly that these two kinds of interactions cannot be considered as separate and additive. Perhaps it would be clearer to think in terms of polar and van der Waals interactions only rather than to invoke a multibody interaction that depends on the complex way that the competition between these two kinds of interactions is resolved. Occam's razor would also argue in favor of the former.

Acknowledgment. We thank the ISIS Pulsed Neutron Facility and the Institut Laue-Langevin for neutron beam time and support facilities.

References and Notes

- (1) Ben-Naim, A. Y. *Hydrophobic Interactions*; Springer Press: Berlin, Germany, 1980; p 205.
- (2) Fernandez-Prini, R.; Corvetto, R. *J. Chem. Phys. Ref. Data* **1989**, *18*, 1231.
- (3) Guillot, B.; Guissani, Y. *J. Chem. Phys.* **1993**, *99*, 8075.
- (4) Iwasaki, K.; Fujiyama, T. *J. Phys. Chem.* **1977**, *81*, 1908.
- (5) Iwasaki, K.; Fujiyama, T. *J. Phys. Chem.* **1979**, *83*, 463.
- (6) Nishikawa, K.; Hayashi, H.; Iijima, T. *J. Phys. Chem.* **1989**, *93*, 6559.
- (7) Franks, F.; Desnoyers, J. E. *Water Sci. Rev.* **1985**, *1*, 171.
- (8) Skipper, N. T.; Bridgeman, C. H.; Buckingham, A. D.; Mancera, R. L. *Faraday Discuss.* **1996**, *103*, 141.
- (9) Mancera, R. L.; Buckingham, A. D. *Chem. Phys. Lett.* **1995**, *234*, 296.
- (10) Pratt, L. R.; Chandler, D. *J. Chem. Phys.* **1977**, *67*, 3683.
- (11) Finney, J. L.; Bowron, D. T.; Daniel, R. M.; Timmins, P.; Roberts, M. A. *Biophys. Chem.* **2003**, *105*, 391.
- (12) Armitage, D. A.; Blandamer, M. J.; Morcom, K. W.; Treloar, N. C. *Nature* **1968**, *219*, 718.
- (13) Bowron, D. T.; Finney, J. L. *Phys. Rev. Lett.* **2002**, *89*, 215508.
- (14) Bowron, D. T.; Finney, J. L. *J. Chem. Phys.* **2003**, *118*, 8357.
- (15) Bowron, D. T.; Finney, J. L.; Soper, A. K. *J. Phys. Chem. B* **1998**, *102*, 3551.
- (16) Bowron, D. T.; Finney, J. L.; Soper, A. K. *J. Chem. Phys.* **2001**, *114*, 6203.
- (17) Finney, J. L.; Soper, A. K. *Chem. Soc. Rev.* **1994**, *23*, 1.
- (18) Soper, A. K.; Howells, W. S.; Hannon, A. C. *ATLAS-Analysis of Time-of-Flight Diffraction Data from Liquid and Amorphous Samples*; Rutherford Appleton Laboratory Report RAL-89-046; Rutherford Appleton Laboratory: Didcot, U.K., 1989.
- (19) Soper, A. K.; Luzar, A. *J. Chem. Phys.* **1992**, *97*, 1320.
- (20) Soper, A. K. *Chem. Phys.* **1996**, *202*, 295.
- (21) Dixit, S.; Soper, A. K.; Finney, J. L.; Crain, J. *Europhys. Lett.* **2002**, *59*, 377.
- (22) Svischev, I. M.; Kusalik, P. G. *J. Chem. Phys.* **1993**, *99*, 3049.
- (23) Finney, J. L.; Bowron, D. T. In *From Semiconductors to Proteins: Beyond the Average Structure*; Billinge, S. F.; Thorpe, M. F., Eds.; Kluwer Academic/Plenum: Dordrecht, The Netherlands, 2002; p 219.
- (24) Finney, J. L. *Proc. R. Soc. London, A* **1970**, *319*, 479.
- (25) Finney, J. L. *Proc. R. Soc. London, A* **1970**, *319*, 495.
- (26) Finney, J. L. *J. Comput. Phys.* **1979**, *32*, 137.